



# Biophotonics of Native Silk Fibrils

Ulyana Shimanovich, Dorothea Pinotsi, Klimentiy Shimanovich, Na Yu, Sreenath Bolisetty, Jozef Adamcik, Raffaele Mezzenga, Jerome Charmet, Fritz Vollrath, Ehud Gazit, Christopher M. Dobson, Gabriele Kaminski Schierle, Chris Holland, Clemens F. Kaminski,\* and Thomas P. J. Knowles\*

Native silk fibroin (NSF) is a unique biomaterial with extraordinary mechanical and biochemical properties. These key characteristics are directly associated with the physical transformation of unstructured, soluble NSF into highly organized nano- and microscale fibrils rich in  $\beta$ -sheet content. Here, it is shown that this NSF fibrillation process is accompanied by the development of intrinsic fluorescence in the visible range, upon near-UV excitation, a phenomenon that has not been investigated in detail to date. Here, the optical and fluorescence characteristics of NSF fibrils are probed and a route for potential applications in the field of self-assembled optically active biomaterials and systems is explored. In particular, it is demonstrated that NSF can be structured into autofluorescent microcapsules with a controllable level of  $\beta$ -sheet content and fluorescence properties. Furthermore, a facile and efficient fabrication route that permits arbitrary patterns of NSF microcapsules to be deposited on substrates under ambient conditions is shown. The resulting fluorescent NSF patterns display a high level of photostability. These results demonstrate the potential of using native silk as a new class of biocompatible photonic material.

is produced in multiple unrelated organisms,<sup>[3]</sup> ranging from ants to spiders, with one of the most prevalent examples being the silkworm *Bombyx mori* (*B. mori*). The *B. mori* silkworm spins fibers from a precursor solution of liquid silk protein, stored in the animal's silk gland, and uses them to form a nonwoven composite cocoon protecting the animal during its further metamorphosis.<sup>[4]</sup> The silk fiber formation process exerts shear and elongation stresses on a concentrated solution containing fibroin (up to 30% wt/vol) in the gland, causing soluble fibroin to denature and aggregate.<sup>[5]</sup> Many studies have been conducted on different types of silk, including the characterization of the structural nature of fibroin,<sup>[6,7]</sup> the aggregation and fiber formation pathway,<sup>[8]</sup> as well as the mechanical and rheological properties of silk solutions and fibers.<sup>[9–11]</sup>

These studies have shown that the molecular architecture of fibrous silk assemblies and the associated irreversible aggregation processes are similar to those found for highly ordered amyloid fibrils.<sup>[12–14]</sup> As functional materials, silk fibroin (SF) fibers are of particular interest because of their

## 1. Introduction

Among all fibrous proteins, native silk fibroin (NSF) has attracted special attention due to its unique properties including mechanical strength, elasticity, and biocompatibility.<sup>[1,2]</sup> Silk

is produced in multiple unrelated organisms, ranging from ants to spiders, with one of the most prevalent examples being the silkworm *Bombyx mori* (*B. mori*). The *B. mori* silkworm spins fibers from a precursor solution of liquid silk protein, stored in the animal's silk gland, and uses them to form a nonwoven composite cocoon protecting the animal during its further metamorphosis.

Dr. U. Shimanovich  
Department of Materials and Interfaces  
Weizmann Institute of Science  
Rehovot 7600, Israel

Dr. D. Pinotsi,<sup>[†]</sup> N. Yu, Dr. G. Kaminski-Schierle, Prof. C. F. Kaminski  
Department of Chemical Engineering and Biotechnology  
University of Cambridge  
Philippa Fawcett Drive  
Cambridge CB3 0AS, UK  
E-mail: cfk23@cam.ac.uk

Dr. K. Shimanovich  
The School of Electrical Engineering  
University of Tel-Aviv, Tel-Aviv 69978, Israel

© 2018 The Authors. Published by WILEY-VCH Verlag GmbH & Co. KGaA, Weinheim. This is an open access article under the terms of the Creative Commons Attribution License, which permits use, distribution and reproduction in any medium, provided the original work is properly cited.  
The copyright line was changed 16 April 2018 after initial publication.

<sup>[†]</sup>Present address: ScopeM Scientific Center for Optical and Electron Microscopy, ETH Zurich, Otto-Stern Weg 3, 8093 Zurich, Switzerland

<sup>[††]</sup>Present address: Institute of Digital Healthcare, WMG, University of Warwick, Coventry CV4 7AL, UK

DOI: 10.1002/mabi.201700295

Dr. S. Bolisetty, Dr. J. Adamcik, Prof. R. Mezzenga  
Department of Health Science and Technology  
ETH Zurich, 8092 Zurich, Switzerland

Dr. J. Charmet,<sup>[††]</sup> Prof. C. M. Dobson, Prof. T. P. J. Knowles  
Department of Chemistry  
University of Cambridge  
Lensfield Road, Cambridge CB2 1EW, UK  
E-mail: tpjk2@cam.ac.uk

Prof. F. Vollrath  
Department of Zoology  
University of Oxford  
South Parks Road, Oxford OX1 3PS, UK

Prof. E. Gazit  
Department of Molecular Biology and Biotechnology  
University of Tel-Aviv, Tel-Aviv 69978, Israel

Prof. E. Gazit  
Department of Materials Science and Engineering  
University of Tel Aviv, Tel Aviv 69978, Israel

Dr. C. Holland  
Department of Materials Science and Engineering  
University of Sheffield, Sheffield S1 3JD, UK

Prof. T. P. J. Knowles  
Cavendish Laboratory  
Department of Physics  
University of Cambridge  
J J Thomson Avenue, Cambridge CB3 0HE, UK

inherent mechanical properties and their compatibility with biological systems.<sup>[15–18]</sup> Although the properties and applications of chemically resolubilized reconstituted silk fibroin (RSF) have been studied extensively in the past,<sup>[19–22]</sup> very little is known about the properties of NSF, in large part because of the inherent difficulties in working with the highly aggregation-prone precursor NSF protein solution of.<sup>[23]</sup> A better understanding of NSF is also for research on synthetic analogs of the protein—so far, the important properties of native silk protein have not been possible to match with synthetic materials.

In this work, we set out to explore the link between NSF aggregation and its emergent structural and intrinsic fluorescence properties. We examined the aggregation of soluble NSF under various destabilizing conditions and found that the transformation of native silk from a disordered random coil to highly ordered-rich  $\beta$ -sheet-rich structure is accompanied by the conformation appearance of a fluorescence signal in the blue–green region of the visible spectrum, which features a long fluorescence lifetime (**Figure 1**). Interestingly, the observed spectral and lifetime characteristics are very similar to those reported for amyloid fibrils, such as amyloid- $\beta$ , lysozyme, and  $\alpha$ -synuclein,<sup>[24–29]</sup> suggesting that there is a common structural origin for the intrinsic fluorescence in NSF and in amyloid fibrils,<sup>[29–32]</sup> independent on the presence of a chemical chromophore. Moreover, we show that aggregation of native silk produces a material with remarkably strong and stable fluorescence characteristics. These features could inspire the next generation of novel photonic structures derived from natural materials. As proof of concept, we demonstrate a possible fabrication route for such systems using microfluidic droplet technology. We show that structuring NSF, contained in microcapsules and subjected to differential microfluidic shear forces, leverages the fluorescence properties of the material and creates a platform for the controlled structuring of aggregation-prone protein materials in general.<sup>[23]</sup>

## 2. Results and Discussion

### 2.1. Intrinsic fluorescence of NSF

We first investigated the fundamental fluorescence properties of fibrillar NSF assemblies. Our results shown in Figure 1a reveal that the transition of native *B. mori* silk protein from the unfolded, soluble state to fibrillar aggregates is accompanied by the appearance of a distinct fluorescence signature that features an excitation maximum at 405 nm and an emission peak at 450 nm (Figure 1b,c). This allows the aggregation process to be monitored by utilizing the intrinsic fluorescence of NSF fibrils. We observed an increase in the fluorescence signal during NSF aggregation (Figure 1d), the kinetics of which correlated with the initial protein concentration. For example, at concentrations below 10 mg mL<sup>−1</sup>, the NSF fluorescence reached its maximum intensity after 1 h of aggregation, as shown in Figure 1d, while at higher concentrations the maximum intensity was reached after 15 min. The fluorescence lifetime of the intrinsic NSF fibril fluorescence was measured using Time Correlated Single Photon Counting (TCSPC) and found to be around 3.5 ns for all the individually observed aggregates (Figure 1e). This value is similar to that found in conventional high quantum yield

fluorescent systems such as dye molecules, quantum dots, and proteins such as green fluorescent protein (GFP) (see table in Figure S1a in the Supporting Information).

To gain insights into the possible physicochemical origin of the intrinsic fluorescence of a variety of NSF fibrils, we exposed soluble NSF to different destabilizing conditions, including: varying pH, mechanical stress or perturbation by continuous shaking, elevated temperature, and different ionic strength and pH conditions. We followed the corresponding conformational changes by using Fourier transform infrared (FTIR) spectroscopy (Figures S1c–f and S2a, Supporting Information) and, depending on the conditions used, discerned possible pathways for the transformation of NSF into fibers. For buffer solutions at pH 4, as well as for physiological buffer conditions (pH = 7 and  $130 \times 10^{-6}$  M of NaCl) and elevated temperature (65 °C) the NSF undergoes a transition from a disordered random coil to a highly ordered structure rich in  $\beta$ -sheet (see FTIR spectra in Figure S1c–f, Supporting Information).<sup>[33]</sup> Interestingly, the percentage of fibrillar content gradually decreases at pH  $\geq 6$ , and below and for conditions of low salt concentration ( $30 \times 10^{-6}$  M NaCl). In particular, pH  $\geq 8$ , the native protein loses fully its ordered structure, and at pH  $\leq 2$ , the NSF exhibits  $\alpha$ -helical,  $\beta$ -sheet as well as random coil character (Figure S1e,f, Supporting Information). Moreover, the intrinsic fluorescence properties of fibrillar silk are identical at pH values of 6, 7, and 8, as well as for fibrils formed at elevated temperatures, under mechanical stress and in aqueous solution of salt concentration corresponding to  $130 \times 10^{-6}$  M of NaCl (Figure S1b, Supporting Information). By contrast, the fibrils formed at pH 4 or at low salt concentration ( $30 \times 10^{-6}$  M NaCl) exhibited a blue shift for both the excitation and the emission spectra (Figure S2b, Supporting Information), with a significant decrease in the corresponding fluorescence intensities. These differences are likely to reflect both changes in the electrostatic environment surrounding the fibrils as well as structural variations in the NSF aggregates.<sup>[33]</sup> Indeed, electrophoretic mobility measurements (Figure S3, Supporting Information) revealed that the surface charge of the NSF fibrils increased from negative to positive with decreasing pH. Notably, at pH 4 under low salt conditions, for which spectral blue shifts were observed, there were two populations of aggregates with two different zeta potential values (Figure S3b, Supporting Information). Overall, therefore, these observations suggest that changes in the surface charge along the protein chain, which is affected by the solution surrounding the fibrils, plays an important role in its fluorescence characteristics, a result that was similarly found for amyloid fibrils.<sup>[29]</sup>

### 2.2. Mechanism of NSF Fibrillation

We monitored the kinetics of NSF fiber formation under different pH conditions but similar protein concentrations, utilizing the NSF intrinsic fluorescence (Figure S2a,d, Supporting Information). We found that lower pH conditions favored faster increases in the fluorescence signal. Moreover, NSF fibrils which formed under more acidic conditions (below pH 4), aggregated faster than at pH 4 and, 7 and at  $30 \times 10^{-6}$  M NaCl solution conditions. The aggregation kinetics were also measured with a Thioflavin-T fluorescence assay (see Figure S4, Supporting

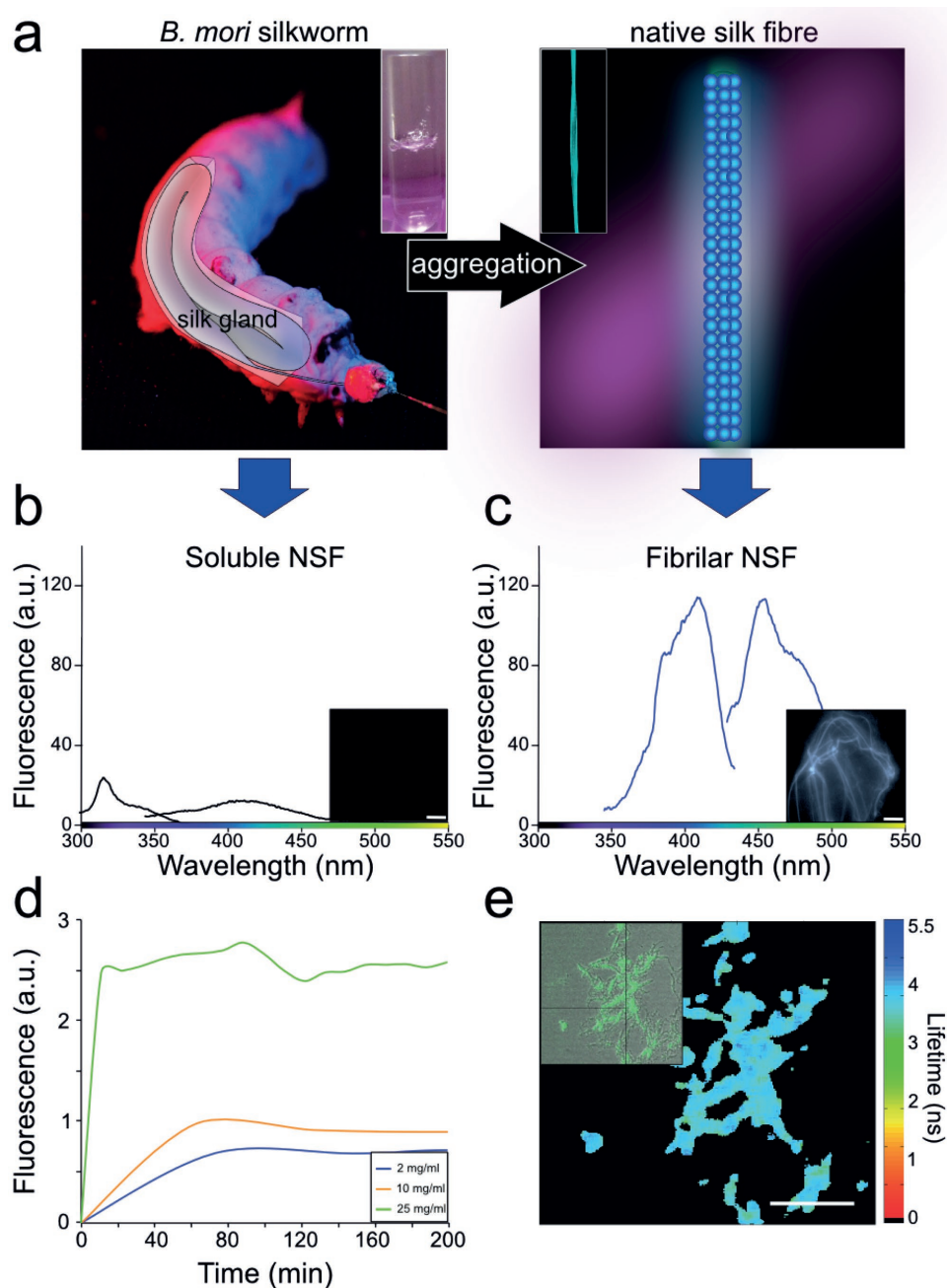


**Figure 1.** a) Image of *B. mori* silkworm (left) and schematic representation of a native silk fibre (right). The insets show images of soluble NSF that was extracted directly from the *B. mori* silkworm gland (left) and aggregated NSF on the right, exhibiting its fibrillar nature. Fluorescence spectra of b) soluble and c) aggregated NSF. The latter exhibits distinct excitation and emission peaks at 405 and 450 nm, respectively. The corresponding fluorescence microscopy images are shown as insets. Scale bars = 5  $\mu$ m. d) Evolution of the intrinsic NSF fluorescence as a function of aggregation time and protein concentration. (e) Inset: overlay of differential interference contrast (DIC) and intrinsic fluorescence images of NSF aggregates in bulk solution. Main panel: fluorescence lifetime image for the same field of view. Images were obtained with a confocal microscope with TCSPC capability using a laser excitation wavelength of 405 nm and a detection window of 50 nm centered at 475 nm. Scale bar = 10  $\mu$ m.

Information), which confirmed that acidic conditions favor the formation of NSF fibrils in comparison to neutral (pH 7) and basic (pH above 7) environments. We then measured the intrinsic fluorescence lifetimes of the fibrils and found that NSF aggregates formed in aqueous solution at neutral pH 7 exhibited shorter lifetimes than those formed under acidic

conditions (Figure S2d, Supporting Information), which is likely reflective of changes in the electrostatic environment, that may both influence fluorescence properties and the NSF fibril structure.

To obtain more detailed insights into the processes of NSF fibrillation and the concurring appearance of the fluorescence

signal, we performed differential scanning calorimetry (DSC), thermogravimetric analysis (TGA) and small-angle wide-angle X-ray scattering (SAXS and WAXS) analysis. The TGA and DSC analysis of the NSF fibers was used to reveal the mechanism of fiber formation, where the thermal degradation stages of the NSF fibers were interpreted as fibrillation stages in the reverse order. First, we investigated the NSF transition from native state to a disordered state after dehydration, and subsequently to the final fibrillar conformation. The analysis of thermal stability of the NSF fibers via thermal degradation, Figure S5c (Supporting Information), showed a distinct weight loss in three main decomposition: small weight loss, beginning at 100 °C and attributed to water evaporation, followed by thermal degradation (at 130 and 140 °C) with significant weight loss (~80%). When compared to TGA analysis, the DSC peak at 150 °C (Figure S5d, Supporting Information) highlights a transition point in the protein conformation, signifying the onset of fast fibrillation. The fibroin chains in the amorphous regions become more and more dense beyond 150 °C, due to breakage and rapid reformation of inter- and intramolecular hydrogen bonds. These data reveal that the NSF folding transitions and fibrillation processes are strongly correlated with the development of the fluorescence properties. We conclude that shortly after water evaporation, NSF reaches an instability point, where molecular reconfiguration and rapid protein aggregation ensues.

### 2.3. Structural Analysis of NSF

We used SAXS and WAXS to examine the structural features of NSF fibers formed under different destabilizing conditions (Figure S6, Supporting Information). The study revealed a hierarchical structural organization of NSF fibers formed in aqueous solutions for pH varying from 2 to 7, displayed by a slope in the scattering vector  $q$  of  $-1.66$ . This value is indicative of protein self-assembly into semi-flexible cylindrical aggregates.<sup>[34]</sup> The WAXS analysis (Figure S6b,c, Supporting Information) revealed two characteristic peaks, one with a  $d$ -spacing of 4.7 Å, which indicates an axial reflection of the inter-strand spacing in the cross- $\beta$  structure and another of 10 Å, corresponding to the equatorial reflection between the  $\beta$ -sheets stacked in the fiber. Similar features are also found in amyloid fibrils.<sup>[10,34]</sup>

The potential for developing functional structures with native silk is determined both by the intrinsic properties of the native protein as well as by the possibility to control the silk fibrillation processes. In order to achieve this control and to explore the effect of such processes on NSF fluorescence, we used a microfluidics approach to generate silk microcapsules. Microfluidics can recapitulate aspects of the natural silk spinning process due to its ability to generate and manipulate fluid flows over small length and volumetric scales.<sup>[35,36]</sup> We thus synthesized silk microcapsules at a T-junction in a microfluidic device (Figure 2a) by emulsifying aqueous silk in an immiscible fluorinated oil phase in a microchannel (see the Experimental Section). This procedure led to the formation of monodisperse silk-in-oil microdroplets, in which the NSF progressively converts into its aggregated form near the

aqueous/oil interface. We found that by controlling the aggregation conditions inside the microdroplets/microcapsules (Figure 2b) we were able to tune systematically the fibrillation level of NSF. We then monitored the increase in NSF fibrillar content inside the microcapsules using cryo-scanning electron microscopy and transmission electron microscopy, as shown in Figure 2c,d. We found that the NSF fibrillation processes in the confined environment of the microcapsules was significantly slower relative to that observed in bulk solution. This effect is likely originates from geometrical constraints imposed by the microdroplets,<sup>[37]</sup> in which nucleation and solvent advection are reduced.<sup>[38,39]</sup> We found that NSF aggregation is initiated at the oil/water interface and subsequently propagates inward to the medial part of the microcapsule, as demonstrated schematically in Figure 2a. Furthermore, after storage of the NSF in the microcapsule interior, the protein can be released in its native conformation by rupturing the outer shell (see the Experimental Section). We next examined the intrinsic fluorescence properties of NSF microcapsules (Figure 2e, and Figure S5a,b in the Supporting Information) by following the fluorescence lifetimes as a function of aggregation time. The fluorescence first appears at the shell of the microdroplet and then propagates towards its interior. These observations are consistent with the electron microscopy results and suggest that the initial nucleation sites occur at the microfluidically sheared water/oil interface. The average fluorescence lifetime measured in microcapsules was  $1.08 \pm 0.03$  ns, which is significantly smaller than that observed in bulk solution ( $3.67 \pm 0.13$  ns). This finding could be explained by more effective exclusion of solvent molecules and the formation of denser structures in the bulk solution. A structural analysis of NSF fibrils formed in the microcapsules showed an identical thermal stability and structural signature as those for the bulk NSF fibrils (see Figures S5 and S6, Supporting Information).

We next explored the optical characteristics of NSF fibrils structured in microcapsules and in bulk. For this purpose we produced an NSF-fibril film coated glass substrate by casting aqueous NSF or NSF microcapsules onto a glass substrate.<sup>[40]</sup> The coated substrate demonstrated a characteristic refraction pattern across the visible range (Figure S7a,b, Supporting Information), which was not observed in the uncoated sample. The dried NSF films were as large as 10 cm<sup>2</sup> in area and revealed a high level of transparency (see Figure S7a,b, Supporting Information) of about 90% across the visible range with absorption values ranging from 4 to 10%. Interestingly, we observed a small increase in the absorption values of samples coated with bulk NSF fibrils and NSF microcapsules in the near-infrared region of 900–940 nm, as shown in Figure S7a,b (Supporting Information). These results demonstrate that NSF fibrils as well as NSF microcapsules could be utilized in the development of optical elements for photonic devices.<sup>[41,42]</sup>

### 2.4. NSF Fluorescent Biomaterials

Finally, we demonstrated a potential route for using fibrillar NSF for the development of functional and fluorescent biomaterials,



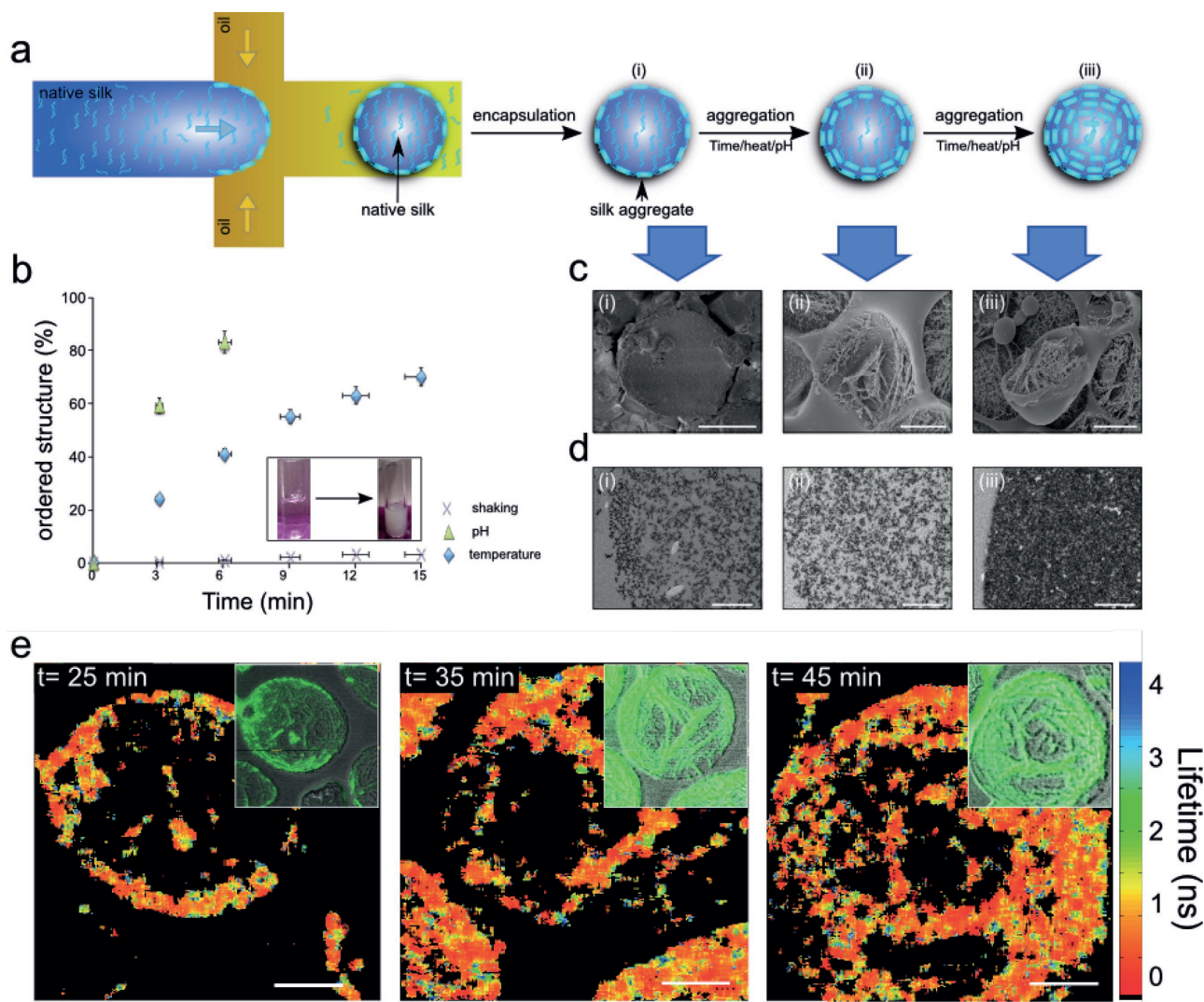


**Figure 2.** a) Schematic representation of microfluidic processing of NSF into microcapsules followed by NSF aggregation within the capsules: (i) non-aggregated state, (ii) partially aggregated NSF microcapsule, and (iii) fully aggregated NSF microcapsule. b) Plot summarizing the silk transformation from disordered random coil to ordered  $\beta$ -sheet rich structure as a function of pH, heating, and perturbation. c) Cryo-scanning electron microscopy images of NSF microcapsules at different aggregation states: (i) non-aggregated state, (ii) partially aggregated NSF microcapsule, and (iii) fully aggregated NSF microcapsule, correspondingly to the scheme shown in (a). Scale bars = 10  $\mu$ m. d) Transmission electron microscopy images of the interior of NSF microcapsules at different aggregation states, which are identical to those shown in scheme (a) and the images from panel (c). Scale bars = 1  $\mu$ m. e) Intrinsic fluorescence lifetime images of NSF microcapsules taken at different time points (from left to right): 25, 35, and 45 min, using confocal microscopy. Insets: overlaid differential interference contrast (DIC) and intrinsic fluorescence images of NSF aggregates inside the microcapsules. The laser excitation was at 405 nm. Scale bars = 10  $\mu$ m.

in a proof-of-concept experiment: We used soft lithography to produce a polydimethylsiloxane (PDMS) microstamp as shown in Figure 3a (see the Experimental Section). This pattern was then filled with either soluble unstructured NSF (Figure 3b), or NSF microcapsules (Figure 3c) and the suspension left to aggregate. During the aggregation process, we recorded the emerging intrinsic fluorescence signal of the fibrillar silk in either bulk or in the microcapsules (Figure 3b,c, and Figure S8 in the Supporting Information). Upon removal of the PDMS device, the fluorescent stamp was then printed onto the glass coverslip, with ink consisting of either fibrillar bulk NSF or NSF microcapsules. We observed a significantly more accurate pattern when using fibrillized NSF microcapsules, due to the

fact that microdroplets can fill in a compartmentalized structure more accurately. Moreover, the stamped NSF patterns exhibited a strong and stable fluorescent signature and showed almost no photobleaching after prolonged light exposure. By contrast, patterns generated with the same device using organic dyes, such as Fluorescein isothiocyanate (FITC), were essentially completely photobleached only after 18 min of exposure for the same conditions (Figure 3d). Moreover, the NSF stamps remained fluorescent, when excited again at 405 nm, after two months of storage at room temperature.

In conclusion, we have investigated the intrinsic fluorescence characteristics of fibrillar NSF and NSF microcapsules along with a potential application route for the development

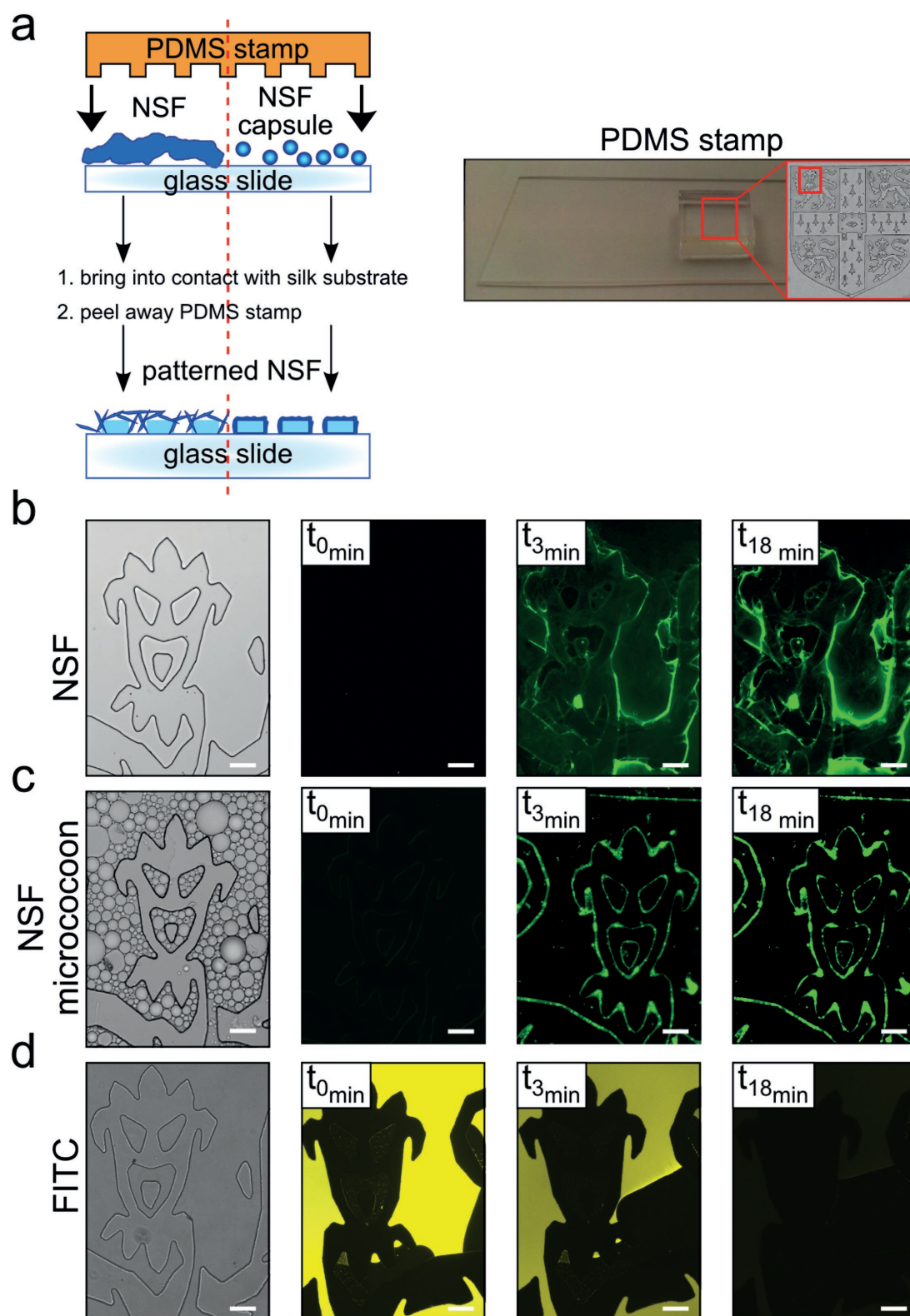


**Figure 3.** Bright field and fluorescence microscopy images of patterned NSF: a) Right: schematic representation of printing fluorescent patterns using native silk and NSF microcapsules. Left: photograph of the patterning stamp with enlarged light microscopy image (right) of the logo of University of Cambridge. b) Images of the pattern filled with native silk and the development of the intrinsic fluorescence signal upon evaporation of solution and subsequent NSF fibrillation. c) Evolution of fluorescence properties for a pattern filled with NSF microdroplets. d) Same pattern formed by FITC. The microscopy images for (c) and (d) were obtained under continuous illumination for 18 min. Scale bars = 20  $\mu\text{m}$ .

of biocompatible photonic devices. In particular, we showed that the properties of the NSF intrinsic fluorescence are directly linked to its fibrillation. The structural characterization of the transformation of the protein from random coil to  $\beta$ -sheet aggregates under ambient as well as destabilizing conditions reveals that the initial nucleation events in aggregation processes are triggered by solvent evaporation, governing the formation of an extensive hydrogen bond network and the appearance of the intrinsic fluorescence signal. This signal increases during aggregation and solvent exclusion until it reaches maximum intensity. The fundamental characteristics of NSF intrinsic fluorescence are comparable to those of standard organic fluorophores, but with greatly increased photostability. Moreover, the structuring of native silk into NSF microcapsules in multi-flow microfluidic platforms enables us to control the aggregation process and fluorescence properties of emerging aggregates. The aggregation-induced optical characteristics of silk together with its biodegradability and biocompatibility may open the door to the development of a new class of functional and fluorescent biomaterials.

### 3. Experimental Section

#### 3.1. Native Silk Feedstock

Native silk samples were extracted from fifth instar *B. mori* larvae during the early stages of cocoon construction as described previously.<sup>[30–32]</sup> In brief, silk glands were removed and the epithelial cells covering the gland were peeled off under cold ( $\approx 5^\circ\text{C}$ ) distilled water, using fine tweezers and a dissection microscope (Olympus SZ 40, Japan). Both posterior sections of the middle division of the silk glands were then placed into a single 2 mL microcentrifuge tube and diluted in distilled water to create 1% W/W native liquid silk solution to be used for processing. *B. mori* silkworms are invertebrates, this study is in accordance with the Animals (Scientific Procedures) Act 1986 of the UK.

#### 3.2. Fluorescence Spectroscopy

The fluorescence spectra of native and aggregated silk in bulk and in the microcapsules were monitored by fluorescence spectroscopy using a Cary Eclipse fluorescent spectrophotometer. The samples were prescanned to calculate the excitation and emission maxima. Then, the emission maximum was confirmed by exciting the samples at wavelengths varying from 300 to 415 nm with intervals of 5 nm for each scan. The excitation maximum was confirmed by measuring at fixed emission wavelengths ranges varying from 400 to 515 nm with an interval of 5 nm for each scan.

#### 3.3. Fluorescence Lifetime Imaging Microscopy

All fluorescence lifetime images were recorded on a home-built confocal microscopy platform based on a confocal microscope scanning unit (Olympus FluoView 300) coupled with an Olympus IX70 inverted microscope frame (Olympus UK). Details can be found in ref. [29].

#### 3.4. Droplet Microfluidics

The following materials were used for preparation of silk microcapsules: native silk protein freshly extracted from *B. mori* silkworm gland and diluted as described above, fluorinert FC-40 (Sigma-Aldrich) and *N,N* bis (*n*-propyl) polyethylene oxide-bis(2-trifluoromethyl polyperfluoroethylene

oxide) amide surfactant. The single T-junction droplet maker PDMS (50 000 Mw) chips was fabricated by a soft lithography method according to an established protocol.<sup>[43]</sup> The synthesis of the NSF microcapsules/microdroplets was performed in a microfluidic device, which consists of channels of 20  $\mu\text{m}$  diameter. Small quantities of immiscible liquid reagents, 1 mL of aqueous NSF and 1 mL of fluorinert oil (fluorinert oil contains 2% surfactant), were mixed on the T-junctions of microfluidic channels by using hydrodynamic pumping. The initial concentration of aqueous (pH = 7) NSF was 10  $\text{mg mL}^{-1}$ . After the microdroplets formation, the capsules were washed with milliQ water in order to remove the surfactant and the unreacted protein residues.

#### 3.5. Generation of the Microfluidic Stamp and Analysis of Its Fluorescence Properties

The PDMS stamp was fabricated using soft-lithography method.<sup>[43]</sup> First, NSF samples (NSF bulk solution or NSF droplets) were deposited onto glass slide. Subsequently, the PDMS stamp was brought into contact with the glass substrate. Finally, the PDMS stamp was removed after the NSF aggregation was completed.

### Supporting Information

Supporting Information is available from the Wiley Online Library or from the author.

### Acknowledgements

U.S. and D.P. contributed equally to this work. The authors thank Nicholas Hawkins for helpful advice regarding NSF aggregation measurements. The authors thank the Swiss National Science Foundation and the Wellcome Trust (C.F.K., D.P.), Elan Pharmaceuticals (C.M.D., T.P.J.K.), the UK BBSRC and ERC (T.P.J.K. and F.V.), the Frances and Augustus Newman Foundation (T.P.J.K.), the AFOSR (F.V.), and EPSRC (C.H. EP/K005693/1, C.F.K.) the MRC (CFK), the Infinitus China Ltd. (CFK), Harold Perlman Family (US), Yad Hanadiv (US), P. and P. Gruber (US), Benozio Center for Advancement of Science (US) and Council for Higher Education-Alon fellowship (US) for the financial support.

### Conflict of Interest

The authors declare no conflict of interest.

### Keywords

biomaterials, intrinsic fluorescence, microfluidics, native silk fibroin, protein fibers

Received: August 30, 2017

Revised: October 18, 2017

Published online: January 29, 2018

- [1] Z. Shao, F. Vollrath, *Nature* **2002**, 418, 741.
- [2] C. Vepari, D. Kaplan, *Prog. Polym. Sci.* **2007**, 32, 991.
- [3] F. Vollrath, D. Porter, C. Holland, *MRS Bull.* **2013**, 38, 73.
- [4] H.-J. Jin, D. L. Kaplan, *Nature* **2003**, 424, 1057.
- [5] F. Vollrath, D. P. Knight, *Nature* **2001**, 410, 541.
- [6] R. E. Marsh, R. B. Corey, L. Pauling, *Biochim. Biophys. Acta* **1955**, 16, 1.
- [7] T. Asakura, J. Ashida, T. Yamane, T. Kameda, Y. Nakazawa, K. Ohgo, K. Komatsu, *J. Mol. Biol.* **2001**, 306, 291.





- [8] M. Boulet-Audet, A. E. Terry, F. Vollrath, C. Holland, *Acta Biomater.* **2014**, *10*, 776.
- [9] M. Heim, D. Keerl, T. Scheibel, *Angew. Chem., Int. Ed.* **2009**, *48*, 3584.
- [10] S. Ling, C. Li, J. Adamcik, Z. Shao, X. Chen, R. Mezzenga, *Adv. Mater.* **2014**, *26*, 4569.
- [11] T. P. J. Knowles, M. J. Buehler, *Nat. Nanotechnol.* **2011**, *6*, 469.
- [12] U. Slotta, S. Hess, K. Spies, T. Stromer, L. Serpell, T. Scheibel, *Macromol. Biosci.* **2007**, *7*, 183.
- [13] C. Dicko, J. M. Kenney, F. Vollrath, *Adv. Protein Chem.* **2006**, *73*, 17.
- [14] J. M. Kenney, D. Knight, M. J. Wise, F. Vollrath, *Eur. J. Biochem.* **2002**, *269*, 4159.
- [15] X. Tang, F. Ding, Y. Yang, N. Hu, H. Wu, X. Gu, *J. Biomed. Mater. Res., Part A* **2009**, *91*, 166.
- [16] C. G. Glabe, R. Kaye, *Neurology* **2006**, *66*, S74.
- [17] U. Shimanovich, I. Efimov, T. O. Mason, P. Flagmeier, A. K. Buell, A. Gedanken, S. Linse, K. S. Åkerfeldt, C. M. Dobson, D. A. Weitz, T. P. Knowles, *ACS Nano* **2015**, *9*, 43.
- [18] X.-M. Zhou, U. Shimanovich, T. W. Herling, S. Wu, C. M. Dobson, T. P. J. Knowles, S. Perrett, *ACS Nano* **2015**, *9*, 5772.
- [19] D. N. Rockwood, R. C. Preda, T. Yucel, X. Wang, M. L. Lovett, D. L. Kaplan, *Nat. Protocols* **2011**, *6*, 1612.
- [20] U. Shimanovich, G. J. L. Bernardes, T. P. J. Knowles, A. Cavaco-Paulo, *Chem. Soc. Rev.* **2014**, *43*, 1361.
- [21] J. G. Hardy, T. R. Scheibel, *Prog. Polym. Sci.* **2010**, *35*, 1093.
- [22] I. Georgakoudi, I. Tsai, C. Greiner, C. Wong, J. DeFelice, D. Kaplan, *Opt. Express* **2007**, *15*, 1043.
- [23] U. Shimanovich, F. S. Ruggeri, E. De Genst, J. Adamcik, T. P. Barros, D. Porter, T. Müller, R. Mezzenga, C. M. Dobson, F. Vollrath, C. Holland, T. P. J. Knowles, *Nat. Commun.* **2017**, *8*, 15902.
- [24] A. Shukla, S. Mukherjee, S. Sharma, V. Agrawal, K. V. Radha Kishan, P. Guptasarma, *Arch. Biochem. Biophys.* **2004**, *428*, 144.
- [25] S. Sharpe, K. Simonetti, J. Yau, P. Walsh, *Biomacromolecules* **2011**, *12*, 1546.
- [26] L. L. Del Mercato, P. P. Pompa, G. Maruccio, A. Della Torre, S. Sabella, A. M. Tamburro, R. Cingolani, R. Rinaldi, *Proc. Natl. Acad. Sci. USA* **2007**, *104*, 18019.
- [27] D. Pinotsi, A. K. Buell, C. M. Dobson, G. S. Kaminski Schierle, C. F. Kaminski, *ChemBioChem* **2013**, *14*, 846.
- [28] F. T. Chan, D. Pinotsi, G. Kaminski Schierle, C. F. Kaminski, in *Bionanoinmaging: Protein Misfolding & Aggregation* (Eds: V. N. Uversky, Y. L. Lyubchenko), Academic Press, San Diego, CA **2014**.
- [29] D. Pinotsi, L. Grisanti, P. Mahou, R. Gebauer, C. Kaminski, A. Hassanali, G. S. Kaminski Schierle, C. F. Kaminski, *J. Am. Chem. Soc.* **2016**, *138*, 3046.
- [30] P. R. Laity, C. Holland, *Biomacromolecules* **2016**, *17*, 2662.
- [31] P. Laity, S. Gilks, C. Holland, *Polymer* **2015**, *67*, 28.
- [32] P. R. Laity, C. Holland, *Int. J. Mol. Sci.* **2016**, *17*, 1812.
- [33] C. W. P. Foo, E. Bini, J. Hensman, D. Knight, R. Lewis, D. Kaplan, *Appl. Phys. A* **2005**, *82*, 223.
- [34] C. Lara, S. Gourdin-Bertin, J. Adamcik, S. Bolisetty, R. Mezzenga, *Biomacromolecules* **2012**, *13*, 4213.
- [35] D. Link, S. Anna, D. Weitz, H. Stone, *Phys. Rev. Lett.* **2004**, *92*, 054503.
- [36] M. E. Kinahan, E. Filippidi, S. Koster, X. Hu, H. M. Evans, T. Pfohl, D. L. Kaplan, J. Wong, *Biomacromolecules* **2011**, *12*, 1504.
- [37] U. Shimanovich, T. P. J. Knowles, C. Holland, WO 2016034730 A1, **2014**.
- [38] T. P. J. Knowles, D. A. White, A. R. Abate, J. J. Agresti, S. I. A. Cohen, R. A. Sperling, E. J. De Genst, C. M. Dobson, D. A. Weitz, *Proc. Natl. Acad. Sci. USA* **2011**, *108*, 14746.
- [39] T. C. T. Michaels, S. I. A. Cohen, M. Vendruscolo, C. M. Dobson, T. P. J. Knowles, *Phys. Rev. Lett.* **2016**, *116*, 038101.
- [40] B. D. Lawrence, M. Cronin-Golomb, I. Georgakoudi, D. L. Kaplan, F. G. Omenetto, *Biomacromolecules* **2008**, *9*, 1214.
- [41] L. Biró, Z. Bálint, K. Kertész, Z. Vértessy, G. Márk, Z. Horváth, J. Balázs, D. Méhn, I. Kiricsi, V. Lousse, J.-P. Vigneron, *Phys. Rev. E* **2003**, *67*, 021907.
- [42] Y.-C. Hung, T.-Y. Lin, W.-T. Hsu, Y.-W. Chiu, Y.-S. Wang, L. Fruk, *Opt. Mater.* **2012**, *34*, 1208.
- [43] B. Zheng, J. D. Tice, L. S. Roach, R. F. Ismagilov, *Angew. Chem., Int. Ed. Engl.* **2004**, *43*, 2508.